University of Groningen

Chaotic dynamics from a pseudo-linear system

Ghane, Hamed; Sterk, Alef E.; Waalkens, Holger

IMPORTANT NOTE: You are advised to consult the publisher's version (publisher's PDF) if you wish to cite from it. Please check the document version below.

Document Version
Publisher's PDF, also known as Version of record

Publication date:
2020

[Link to publication in University of Groningen/UMCG research database](#)

Chaotic dynamics from a pseudo-linear system

Hamed Ghane[*]

*Bernoulli Institute, University of Groningen, PO Box 407, 9700 AK Groningen, The Netherlands and
Bandar Anzali Branch, Islamic Azad University, Bandar Anzali, Iran*
*Corresponding author. Email: Hamed_ghane_s@aut.ac.ir

AND

Alef E. Sterk and Holger Waalkens

Bernoulli Institute, University of Groningen, PO Box 407, 9700 AK Groningen, The Netherlands

Investigating the possibility of applying techniques from linear systems theory to the setting of non-linear systems has been the focus of many papers. The pseudo-linear (PL) form representation of non-linear dynamical systems has led to the concept of non-linear eigenvalues (NEValues) and non-linear eigenvectors (NEVectors). When the NEVectors do not depend on the state vector of the system, then the NEValues determine the global qualitative behaviour of a non-linear system throughout the state space. The aim of this paper is to use this fact to construct a non-linear dynamical system of which the trajectories of the system show continual stretching and folding. We first prove that the system is globally bounded. Next we analyse the system numerically by studying bifurcations of equilibria and periodic orbits. Chaos arises due to a period doubling cascade of periodic attractors. Chaotic attractors are presumably of Hénon-like type, which means that they are the closure of the unstable manifold of a saddle periodic orbit. We also show how PL forms can be used to control the chaotic system and to synchronize two identical chaotic systems.

Keywords: chaos generation; qualitative analysis; pseudo-linear systems; non-linear eigenvalues; non-linear eigenvectors.

1. Introduction

The analysis of non-linear systems is a wide field of research with many applications and techniques. One main approach to the analysis and control of non-linear systems consists of transferring results from linear systems theory. The best known example is the Poincaré linearization near an equilibrium point where for a hyperbolic equilibrium point, the linear dynamics associated with the Jacobian matrix of the vector field is by the Hartman–Grobman theorem conjugate to the non-linear dynamics near the equilibrium point; see, e.g. Cheng *et al.* (2010). As another linearization scheme we mention feedback linearization that amounts to designing a feedback control along with some change of coordinate that transforms the closed-loop non-linear system into a linear system; see Baillieul & Willems (1999).

However, one of the most effective applications of linear systems theory in non-linear systems is the state-dependent Riccati equation (SDRE) strategy in non-linear optimal control theory; see Çimen (2008). This approach requires a representation of the non-linear dynamics into a linear form with a state-dependent system matrix. In doing so, this matrix-valued function fully captures the

non-linearities of the system, which provides the designer a very effective method of making a good and yet systematic trade-off between state error and input effort via a state-dependent linear quadratic formulation. An SDRE, of which the coefficients vary across state space, is then solved to give a suboptimal control law. The SDRE approach in non-linear optimal control design relies on the pseudo-linear (PL) representation of a non-linear dynamical system. Indeed, the closed-loop system obtained by this optimal controller is still in a PL form. However, the stability analysis of the closed-loop system by exerting the resulting optimal control is still a problematic challenge and has attracted several studies during the past years. As noted by Cloutier (1997), the number of successful applications of the SDRE approach in the design of non-linear optimal controllers outpaced the available theoretical results.

Investigating the possibility of using the PL form representation in the stability analysis of non-linear systems has been the effort of several works, e.g. Banks & Mhana (1992, 1996), Tsiotras *et al.* (1996), Langson & Alleyne (2002) and Muhammad & Van Der Woude (2009). The key focus of these works was the stabilizability of a PL form by exerting the state-dependent control obtained via the SDRE approach. Recently, Ghane & Menhaj (2015) introduced a theorem providing a sufficient condition of a PL system for correct stability analysis based on its state-dependent eigenvalues and eigenvectors. Although the PL representation was originally introduced for the systematic design of a non-linear optimal controller through the SDRE approach, Ghane & Menhaj (2015) have shown that besides stability analysis, the PL form can also provide a useful tool for the global qualitative analysis of non-linear dynamical systems when the non-linear eigenvectors (NEVectors) obtained from this PL representation are state-independent (SI).

The ability of determining the qualitative behaviour of a non-linear dynamical system by means of eigenvalues and eigenvectors obtained from a PL form is also attractive for fields beyond control engineering applications, such as dynamical systems (see Ghane & Menhaj, 2014). The widespread applications of chaotic systems in practical applications, like image watermarking (see Wang *et al.*, 2015), chaotic communication (see Zhou *et al.*, 2014 and Çiçek *et al.*, 2016) and robotics (see Zang *et al.*, 2016), have motivated us to apply this qualitative approach to generate a class of chaotic systems. In this paper, we apply the PL representation in the interesting field of chaos generation that may be potentially useful for the engineering applications mentioned above.

The aim of this paper is to synthesize the basic qualitative characteristics of a chaotic behaviour. With the help of non-linear eigenvalues (NEValues) as the qualitative indicator of the behaviour of a system in PL form, we introduce a system with a specific type of locally unstable and globally bounded trajectories. The system that we construct in this way has equilibria that become unstable through a Hopf bifurcation. The resulting periodic orbits bifurcate further through a period doubling cascade that leads to chaotic attractors. The latter are presumably of Hénon-like type, which means that they are the closure of the unstable manifold of a saddle periodic orbit. In addition, we show the application of NEValues in non-linear control and synchronization of the chaotic system.

The rest of the paper is organized as follows. In Section 2, the PL representation of non-linear systems is briefly introduced and its ability for qualitative analysis of non-linear dynamical systems is discussed. Section 3 is devoted to use the PL form to generate a chaotic system and to prove the global boundedness of the trajectories. The dynamical analysis of the obtained chaotic system is presented in Section 4. In Section 5, an eigenstructure-based analysis is used to design a control law for the chaotic system and to perform an identical synchronization of two chaotic systems. Finally, some concluding remarks are presented in Section 6.

2. PL systems: a brief review

An autonomous non-linear system is described by a system of non-linear ordinary differential equations that do not explicitly depend on the independent variable. The general form of such a system is given by

$$\dot{\mathbf{x}}(\mathbf{t}) = \mathbf{f}(\mathbf{x}(\mathbf{t})), \tag{2.1}$$

where $\mathbf{x}$ takes values in n-dimensional Euclidean space and the independent variable t is usually time. Now assume that $\mathbf{f} : \mathbb{R}^\mathbf{n} \to \mathbb{R}^\mathbf{n}$ is sufficiently smooth and that $\mathbf{f}(\mathbf{0}) = \mathbf{0}$. Inspired by the theory of linear systems we can then transform an autonomous system (2.1) to the form

$$\dot{\mathbf{x}}(t) = A(\mathbf{x}(t))\mathbf{x}(t), \tag{2.2}$$

where $A : \mathbb{R}^n \to \mathbb{R}^{n \times n}$. This form is calledPL and it was originally introduced by Banks & Mhana (1992) to cope with the difficulty of designing optimal control laws for non-linear systems.

Using the PL form (2.2), it is possible to extend the concept of eigenvalues and eigenvectors to the setting of non-linear systems. The NEValue and its corresponding NEVector are defined as the functions $\lambda : \mathbb{R}^n \to \mathbb{C}$ and $\mathbf{v} : \mathbb{R}^n \to \mathbb{C}^n$, respectively, that satisfy the equation

$$A(\mathbf{x})\mathbf{v}(\mathbf{x}) = \lambda(\mathbf{x})\mathbf{v}(\mathbf{x}). \tag{2.3}$$

Equivalently, the NEValues can also be obtained as the solution of the characteristic equation

$$\det\left(A(\mathbf{x}) - \lambda(\mathbf{x})I_n\right) = 0. \tag{2.4}$$

Based on these generalized concepts, the following remarks and proposition are presented. Proofs and more explanations can be found in Ghane & Menhaj (2014, 2015). By means of these results we can study the qualitative behaviour of non-linear dynamical systems. The qualitative analysis of non-linear systems based on PL forms mainly uses the following observation from linear systems theory.

REMARK 2.1 The qualitative behaviour of non-linear systems is determined by the following:

1. The sign of the real part of the NEValues;

2. The realness or complexness of the NEValues.

The first condition determines the stability properties of the dynamics and the second condition determines the spiralling or exponential nature.

Consider a non-linear dynamical system $\dot{\mathbf{x}} = \mathbf{f}(\mathbf{x})$, where $\mathbf{f} : \mathbb{R}^\mathbf{n} \to \mathbb{R}^\mathbf{n}$ satisfies $\mathbf{f}(\mathbf{0}) = \mathbf{0}$. Among the infinite distinct possible PL forms of this system, only the unique PL form that hasSI NEVectors must be used in eigenstructure-based analysis, because only a PL form with SI NEVectors is guaranteed to yield correct qualitative results through its NEValues analysis.

PROPOSITION 2.2 For a non-linear system $\dot{\mathbf{x}} = \mathbf{f}(\mathbf{x})$, where $\mathbf{f} : \mathbb{R}^\mathbf{n} \to \mathbb{R}^\mathbf{n}$ satisfies $\mathbf{f}(\mathbf{0}) = \mathbf{0}$, a sufficient condition for global asymptotic stability of the origin is that the system has a PL form representation that satisfies the following conditions:

1. $\mathrm{Re}\left\{\lambda_i(\mathbf{x})\right\} < 0$ for all $\mathbf{x} \in \mathbb{R}^\mathbf{n}$ and $i = 1, \ldots, n$;

2. For every NEValue the algebraic and geometric multiplicities are equal;

3. All NEVectors of the matrix $A(\mathbf{x})$ are SI.

This proposition has been proved through discretization of the non-linear differential equation of the underlying system in Ghane & Menhaj (2014).

All of the aforementioned results are applicable to the special class of non-linear systems of the form (2.2) in which $A(\mathbf{x}) = diag(D_1(\mathbf{x}), \ldots, D_p(\mathbf{x}))$ is a block diagonal matrix and where each block is of the form

$$D_i(\mathbf{x}) = \begin{bmatrix} g_i(\mathbf{x}) \end{bmatrix} \quad \text{or} \quad D_i(\mathbf{x}) = \begin{bmatrix} g_i(\mathbf{x}) & -\omega_i \\ \omega_i & g_i(\mathbf{x}) \end{bmatrix},$$

where $g_i : \mathbb{R}^n \to \mathbb{R}$ and $\omega_i > 0$ for $i = 1, \ldots, p$. Each 1×1 block gives rise to a real NEValue and each 2×2 block gives rise to a complex NEValue. It is straightforward to verify that the corresponding NEVectors are SI.

3. Chaos generation

Qualitatively speaking, the occurrence of chaotic behaviour is usually related to the interplay between local instability and global boundedness of trajectories (see Schöll & Schuster, 2008). The local instability is responsible for the exponential divergence of nearby trajectories, while the global boundedness folds trajectories within the finite volume of the system's phase space. The combination of these two mechanisms can result in high sensitivity of the system trajectories to the initial conditions. In this paper we use NEValues of a PL form as indicators of a system's qualitative behaviour and to construct a dynamical system that shows chaotic behaviour without the need for exhaustive tuning of parameter values.

3.1. *Constructing a candidate chaotic system*

The Poincaré–Bendixson theorem implies that the dynamical behaviour a system of the form (2.1) with $n = 2$ cannot be chaotic; see Guckenheimer & Holmes (1983). Hence, the minimum dimension of a chaotic system is $n = 3$. We first concentrate on finding non-linear functions $\lambda_i(\mathbf{x})$, where $i = 1, 2, 3$, to generate the continual stretching and folding property in the dynamics of the system. By the approach proposed in the previous section, it is possible to produce such a behaviour with a proper selection of NEValues. As a result, this approach may lead to different choices of NEValues that satisfy the desired qualitative behaviour; one of these choices is the following one:

$$
\begin{aligned}
\lambda_{1,2}(\mathbf{x}) &= \left(x_3^2 - h^2\right) \pm j\omega, \\
\lambda_3(\mathbf{x}) &= r^2 - ax_1^2 - bx_2^2 - cx_3^2,
\end{aligned}
\tag{3.1}
$$

in which $a, b, c, \omega, h, r > 0$ are fixed parameters and $j^2 = -1$.

Applying Remark 2.1, these NEValues give rise to the following non-linear system:

$$
\begin{aligned}
\dot{x}_1 &= (x_3{}^2 - h^2)x_1 - \omega x_2, \\
\dot{x}_2 &= \omega x_1 + (x_3{}^2 - h^2)x_2, \\
\dot{x}_3 &= (r^2 - ax_1{}^2 - bx_2{}^2 - cx_3{}^2)x_3.
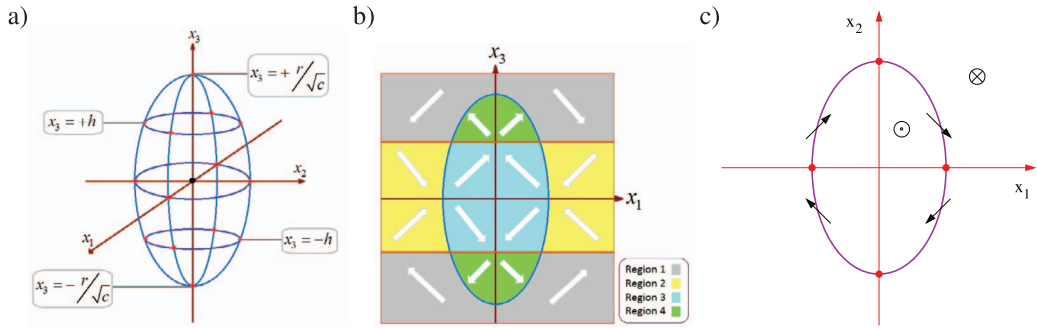\end{aligned}
\tag{3.2}
$$

FIG. 1. Graphical illustration of the qualitative behaviour of system (3.2). On the ellipsoid $ax_1{}^2 + bx_2{}^2 + cx_3{}^2 = r^2$ and on the plane $x_3 = 0$ the x_3-component of the vector field is vanishing. On the planes $x_3 = \pm h$, $\dot{\rho} = 0$. (a) Nullclines $\dot{x}_3 = 0$ and $\dot{\rho} = 0$ in the three-dimensional state space. (b) Section $x_2 = 0$ of the state space. The arrows indicate direction of the vector field in terms of the signs of $\dot{x}_3$ and $\dot{\rho}$ in the regions 1, 2, 3 and 4. (c) Section $x_3 = 0$ with the intersection of the nullclines along the ellipse $ax_1{}^2 + bx_2{}^2 + ch^2 = r^2$. In the region enclosed by the ellipse the x_3-component of the vector field is positive. Outside it is negative. The arrows indicate the direction of the vector field on the ellipse.

The NEVectors of the system (3.2), which are simply given by

$$\mathbf{v_1} = \begin{bmatrix} 1 & -j & 0 \end{bmatrix}^\top, \quad \mathbf{v_2} = \begin{bmatrix} j & 1 & 0 \end{bmatrix}^\top, \quad \mathbf{v_3} = \begin{bmatrix} 0 & 0 & 1 \end{bmatrix}^\top,$$

satisfy the condition of Remark 2.1. Therefore, the chosen NEValues guarantee that the system will exhibit the continual stretching and folding that is characteristic of a chaotic system. For further analysis, it is convenient to set $x_1 = \rho \cos \theta$ and $x_2 = \rho \sin \theta$ by which the system (3.2) can be rewritten in terms of cylindrical coordinates

$$\begin{aligned} \dot{\rho} &= \left(x_3^2 - h^2 \right) \rho, \\ \dot{\theta} &= \omega, \\ \dot{x}_3 &= (r^2 - a\rho^2 \cos^2 \theta - b\rho^2 \sin^2 \theta - cx_3^2)x_3. \end{aligned} \tag{3.3}$$

As illustrated in Fig. 1 the ρ nullclines given by the horizontal planes $x_3 = \pm h$ and the x_3 nullclines given by the ellipsoid $ax_1{}^2 + bx_2{}^2 + cx_3{}^2 = r^2$ and the horizontal plane $x_3 = 0$ divide the state space into four regions with different signs of the real parts of the NEValues that give rise to the different qualitative behaviours described in Table 1. Note that we consider the regions to be open, i.e. to not contain their boundaries. In regions 2 and 4, the real parts of all NEValues are positive and negative, respectively. Thus, in these regions the trajectories of the system are repelled from and attracted to the origin, respectively. In line with our approach for chaos generation, the existence of these two types of behaviours besides the regions 1 and 3 with saddle behaviour is necessary to ensure both the stretching and the folding of system trajectories. A proper arrangement of these regions then guarantees that the trajectories of the system remain bounded, which is proved in detail on the next subsection. This arrangement is assured in system (3.2) by the assistance of the regions 1 and 3.

Observe that replacing x_3 by $-x_3$ in (3.2) yields the same equations. As a consequence the plane $x_3 = 0$ is invariant under the flow. Therefore, it suffices to discuss the dynamics for $x_3 > 0$ and this is what we do for the rest of the paper.

TABLE 1   *Qualitative behaviour of the non-linear system (3.2) based on an analysis of the NEValues*

|	Region	Sign of Re $\{\lambda(\mathbf{x})\}$		Qualitative behaviour
1	$ax_1{}^2 + bx_2{}^2 + cx_3{}^2 > r^2$ $x_3{}^2 > h^2$	Re $\{\lambda_{1,2}(\mathbf{x})\} > 0$	$\frac{\mathrm{d}}{\mathrm{d}t}\rho > 0$	Increasing spiral
		Re $\{\lambda_3(\mathbf{x})\} < 0$	$\frac{\mathrm{d}}{\mathrm{d}t}\left(\lvert x_3\rvert\right) < 0$	Decreasing exponential
2	$ax_1{}^2 + bx_2{}^2 + cx_3{}^2 > r^2$ $x_3{}^2 < h^2$	Re $\{\lambda_{1,2}(\mathbf{x})\} < 0$	$\frac{\mathrm{d}}{\mathrm{d}t}\rho < 0$	Increasing spiral
		Re $\{\lambda_3(\mathbf{x})\} < 0$	$\frac{\mathrm{d}}{\mathrm{d}t}\left(\lvert x_3\rvert\right) < 0$	Decreasing exponential
3	$ax_1{}^2 + bx_2{}^2 + cx_3{}^2 < r^2$ $x_3{}^2 < h^2$	Re $\{\lambda_{1,2}(\mathbf{x})\} < 0$	$\frac{\mathrm{d}}{\mathrm{d}t}\rho < 0$	Increasing spiral
		Re $\{\lambda_3(\mathbf{x})\} > 0$	$\frac{\mathrm{d}}{\mathrm{d}t}\left(\lvert x_3\rvert\right) > 0$	Decreasing exponential
4	$ax_1{}^2 + bx_2{}^2 + cx_3{}^2 < r^2$ $x_3{}^2 > h^2$	Re $\{\lambda_{1,2}(\mathbf{x})\} > 0$	$\frac{\mathrm{d}}{\mathrm{d}t}\rho > 0$	Increasing spiral
		Re $\{\lambda_3(\mathbf{x})\} > 0$	$\frac{\mathrm{d}}{\mathrm{d}t}\left(\lvert x_3\rvert\right) > 0$	Decreasing exponential
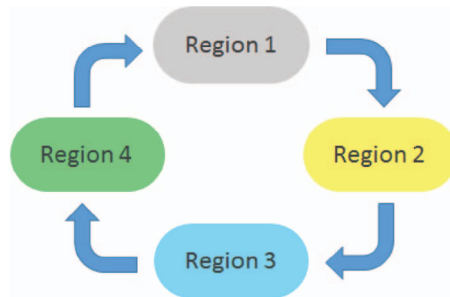
FIG. 2. The cyclic evolution of solution trajectories of the system (3.2).

From the equations of motion (3.2) we see that the x_3-axis is also invariant under the flow. From the third component of (3.2) we see that the plane $x_3 = h$ is transversal to the flow at all points not contained in the intersection with the ellipsoid $ax_1{}^2 + bx_2{}^2 + cx_3{}^2 = r^2$. The ellipsoid $ax_1{}^2 + bx_2{}^2 + cx_3{}^2 = r^2$ is, however, not even away from its intersection with the plane $x_3 = h$ transversal to the flow. Still we can use the structure of the NEValues summarized in Table 1 to infer that the system trajectories with initial conditions $x_3 > 0$ and not contained in the invariant x_3-axis visit the different region in the cyclic pattern illustrated in Fig. 2. To this end first note that the NEValues show that trajectories cannot get permanently trapped in either of the regions 1, 2, 3 or 4. Let us consider trajectories going through the intersection of the nullclines $\dot{\rho} = 0$ and $\dot{x}_3 = 0$ that is given by the ellipse $ax_1{}^2 + bx_2{}^2 + ch^2 = r^2$ in the plane $x_3 = h$. The ellipse is illustrated in Fig. 1(c) for the case $a > b$ (for $a < b$ relabel x_1 and x_2). Trajectories crossing the ellipse in the first or third quadrant evolve from region 3 to region 2. Trajectories crossing the ellipse in the second or fourth quadrant evolve from region 1 to region 4. At the four points on the ellipse contained on the x_1-axis or x_2-axis the vector field is tangent to the ellipse.

At the two points on the ellipse located on the x_1-axis the trajectories evolve from region 3 to region 4. At the two points on the ellipse located on the x_2-axis the trajectories evolve from region 1 to region 2.

Using the above results on how the nullclines $\dot{x}_3 = 0$ and $\dot{\rho} = 0$ are crossed by trajectories we can conclude the following on the evolution between the different regions. All trajectories with initial conditions in region 4 will evolve directly (i.e. without visiting any other region in between) to region 1. Similarly, all trajectories with initial conditions in region 2 will evolve directly to region 3. Trajectories with initial conditions in region 1 evolve directly to region 2 or move to region 2 after a finite number of visits to region 4. The latter option follows from the non-transversality of the boundary between regions 1 and 4 and the fact that ρ is exponentially increasing in regions 1 and 4. Similarly, trajectories with initial conditions in region 3 evolve directly to region 4 or move to region 4 after a finite number of visits to region 3. The latter option follows from the non-transversality of the boundary between regions 2 and 3 and the fact that ρ is exponentially decreasing in regions 2 and 3.

By the arrangement of regions 1–4, it follows that the stretching of trajectories occurs along the x_3-axis followed by the folding action and the cyclic pattern occurs repeatedly. On the other hand, the results of the qualitative analysis of the system trajectories summarized in Table 1 and Figs 1 and 2 suggest that the system will be globally bounded, which will be rigorously proved in the next subsection.

In summary, based on this qualitative analysis we expect that the synthesized system (3.2) will exhibit chaotic behaviour for a suitable range of parameter values. Note that the proposed approach is essentially qualitative without any quantitative rigorous proof. In the next section, we present a numerical analysis of the system that indeed suggests the occurrence of chaotic behaviour and we discuss some interesting features of the system.

3.2. *Boundedness of system trajectories*

We note that all orbits in the plane $x_3 = 0$ are attracted to the origin (see Section 4.1) that guarantees boundedness of trajectories with initial conditions in the plane $x_3 = 0$ in the forward time direction.

Given the possible transport scenarios between the regions 1–4 discussed in the previous subsection the boundedness of system trajectories in general follows from the following proposition.

PROPOSITION 3.1 Trajectories with initial conditions in region 1 can enter region 2 only with a finite maximal value of ρ (where this maximal value depends on the initial condition).

This gives the boundedness of system trajectories in general because of the following (as before we consider because of symmetry only the half $x_3 > 0$):

1. Trajectories on the invariant x_3-axis have $\dot{x}_3 < 0$ for $x_3 > r\sqrt{c}$;

2. Regions 3 and 4 are bounded;

3. Region 2 is bounded in the vertical direction from below and from above and in region 2 we have $\dot{\rho} < 0$; and

4. Region 1 can only be entered from the bounded region 4.

Let us now prove Proposition 3.1.

Proof. (Proposition 3.1) We show that trajectories with initial conditions $(x_1(0), x_2(0), x_3(0)) = (x_{10}, x_{20}, x_{30})$ in region 1 will reach the plane $x_3 = h$ in the forward time direction with a finite value ρ_0. Let $x_{30} = x_3(0)$ and $d = \min\{a, b\} > 0$. Then there exists a $\rho_1 > \max\{r/\sqrt{d}, \sqrt{x_{10}^2 + x_{20}^2}\}$ such that

for all points (x_1, x_2, x_3) with $h \leqslant x_3 \leqslant x_{30}$ and $\sqrt{x_1^2 + x_2^2} = \rho \geq \rho_1$ the following holds: the slope of the projection of the trajectory to the $x_3 - \rho$ coordinate plane that is negative by the definition of region 1 satisfies by the chain rule

$$\frac{\dot{x}_3}{\dot{\rho}} = \frac{(r^2 - ax_1^2 - bx_2^2 - cx_3^2)\, x_3}{(x_3^2 - h^2)\rho} \leqslant \frac{(r^2 - d\rho^2)x_3}{(x_3^2 - h^2)\rho} \tag{3.4}$$

$$\leqslant \frac{(r^2 - d\rho^2)x_3}{(x_{30}^2 - h^2)\rho} \tag{3.5}$$

$$\leqslant \frac{(r^2 - d\rho^2)h}{(x_{30}^2 - h^2)\rho} \tag{3.6}$$

$$< -1. \tag{3.7}$$

Here the inequality in (3.4) uses $r^2 - ax_1^2 - bx_2^2 - cx_3^2 < r^2 - d\rho^2$ that follows by the definition of d and the fact that $\rho > \max\{r/\sqrt{d}, \sqrt{x_{10}^2 + x_{20}^2}\}$. The second and the third inequalities, (3.5) and (3.6), use $x_3 \leq x_{30}$ and $x_3 \geq h$, respectively. The existence of ρ_1 and the last inequality (3.7) follow from the expression in (3.6) going to $-\infty$ as $\rho \to \infty$. As $\dot{x}_3 < 0$ in region 1 the vertical variation of the trajectory in the forward time direction is equal to $x_{30} - h$ before the orbit reaches the plane $x_3 = h$. The orbit can then depart in the forward time direction no further from the x_3-axis than $\rho_0 = \rho_1 + x_{30} - h$ before it reaches the plane $x_3 = h$.   □

4. Dynamical analysis of the candidate system

In this section we study the dynamics of the system (3.2). We start by studying the bifurcations of equilibria and periodic orbits. Numerical simulations suggest that chaotic attractors appear after a cascade of period doubling bifurcations. These chaotic attractors are presumably of Hénon-like type, which means that they are the closure of the unstable manifold of a saddle periodic orbit.

4.1.   *Equilibria and their stability*

For $x_3 \geqslant 0$, the system has the following equilibria:

$$O = (0, 0, 0), \quad Z = (0, 0, r/\sqrt{c}).$$

The eigenvalues of the Jacobi matrix $J = D\mathbf{f}$ evaluated at O are given by

$$\lambda_{O,1} = -h^2 + \omega j, \quad \lambda_{O,2} = -h^2 - \omega j, \quad \lambda_{O,3} = r^2.$$

Under the assumption that $h, r \neq 0$ the stable and unstable manifolds of O are given by

$$W^s(O) = \left\{(x_1, x_2, 0) \in \mathbb{R}^3\right\},$$

$$W^u(O) = \left\{(0, 0, x_3) \in \mathbb{R}^3 \; : \; 0 < |x_3| < r/\sqrt{c}\right\}.$$

The eigenvalues of the matrix J evaluated at Z are given by

$$\lambda_{Z,1} = r^2/c - h^2 + \omega j, \quad \lambda_{Z,2} = r^2/c - h^2 - \omega j, \quad \lambda_{Z,3} = -2r^2.$$
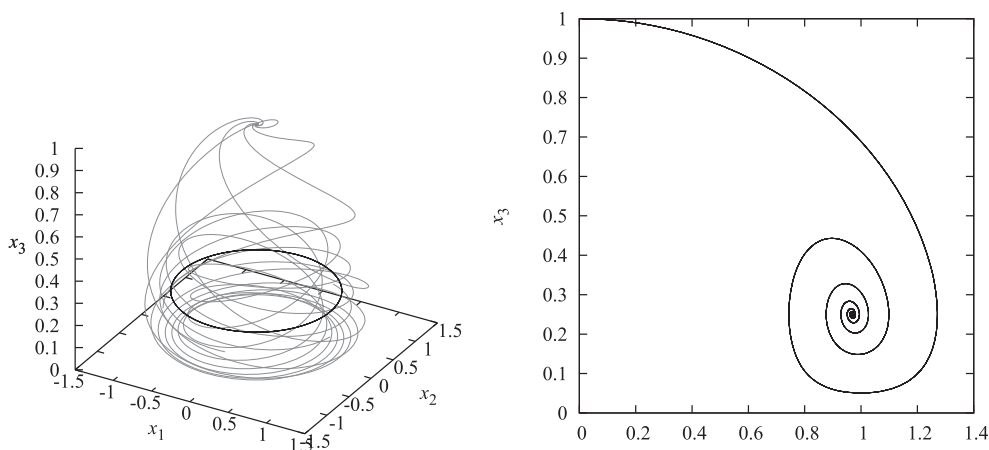
FIG. 3. Left: five orbits on the unstable manifold of the equilibrium Z for the parameters $(a, b, c, h, r, \omega, c) = (1, 1, 1, 0.25, 1, 1)$ (grey) and a stable periodic orbit (black). Right: cross section of the unstable manifold of the equilibrium Z.

Note that the complex eigenvalue pair $(\lambda_{Z,1}, \lambda_{Z,2})$ crosses the imaginary axis when $h = r/\sqrt{c}$. This implies that, under suitable non-degeneracy conditions, the equilibrium Z becomes unstable through a Hopf bifurcation that gives birth to a stable periodic orbit (see Kuznetsov, 2004).

For $a = b$ and $r^2/c - h^2 > 0$ it is straightforward to verify that

$$
\begin{aligned}
x_1(t) &= \rho_0 \cos(\omega t), \\
x_2(t) &= \rho_0 \sin(\omega t), \\
x_3(t) &= h,
\end{aligned}
\tag{4.1}
$$

where $\rho_0 = \sqrt{(r^2 - ch^2)/a}$, is a periodic orbit of the system (3.2). Note that for $h = r/\sqrt{c}$ this orbit coalesces with the equilibrium Z. This suggests that for $a = b$ the periodic orbit in equation (4.1) indeed arises through a Hopf bifurcation of the equilibrium Z.

Under the assumptions that $r \neq 0$ and $r^2/c - h^2 > 0$ it follows that the stable manifold of Z is given by

$$
W^s(Z) = \left\{ (0, 0, x_3) \in \mathbb{R}^3 \, : \, x_3 > 0 \right\}.
$$

The two-dimensional unstable manifold of Z cannot be computed analytically, but the linearization of the system (3.2) at Z shows that the unstable manifold is tangent to the plane $\{(x_1, x_2, r/\sqrt{c}) : x_1, x_2 \in \mathbb{R}\}$. Figure 3 shows a numerical approximation of $W^u(Z)$, which suggests that this manifold is part of the stable manifold of a periodic orbit.

4.2. *Periodic orbits and their bifurcations*

The periodic solutions of (3.2) can be studied in terms of a so-called Poincaré return map (see Guckenheimer & Holmes, 1983). The idea is to study the intersections of orbits of (3.2) with a plane
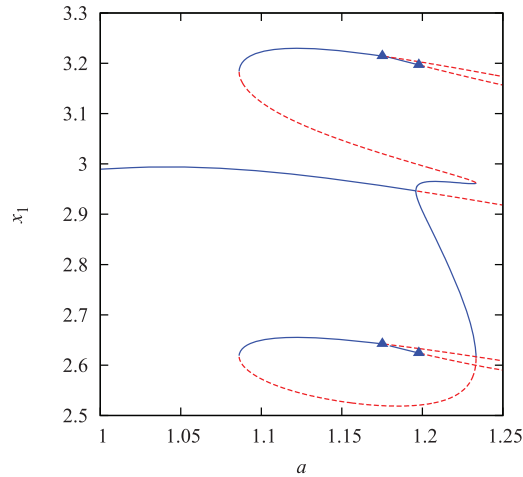
FIG. 4. Bifurcation diagram of fixed points of the Poincaré map $P : \Sigma \to \Sigma$ as a function of the parameter a. The other parameters are fixed at $(b, c, h, r, \omega) = (1, 1, 0.25, 3, 1)$. Blue solid lines indicate stable branches and red dashed lines represent unstable branches. Triangles denote period doubling bifurcations. Note that multiple stable fixed points can coexist for the same parameter values.

that is transversal to the vector field. Consider the following set:

$$\Sigma = \left\{ (x_1, 0, x_3) \in \mathbb{R}^3 : x_1 > 0, \, x_3 > 0 \right\}.$$

We define the Poincaré map $P : \Sigma \to \Sigma$ as follows. If $(x_1, 0, x_3) \in \Sigma$, then $P(x_1, 0, x_3)$ is defined by integrating equation (3.2) for $2\pi / \omega$ units of time. From equation (3.3) it follows that indeed $P(\Sigma) \subset \Sigma$. In addition, the existence and uniqueness theorems for differential equations imply that the map P is a diffeomorphism. A point $\mathbf{x} \in \Sigma$ is called a period-n point of P if $P^n(\mathbf{x}) = \mathbf{x}$. Such points correspond to periodic orbits of (3.2) that make n turns around the x_3-axis. Period-1 points of P are also referred to as fixed points of P.

For $a = b$ and $r^2/c - h^2 > 0$, the point $(\rho_0, 0, h)$, with $\rho_0 = \sqrt{(r^2 - ch^2)/a}$, is a fixed point of the map P. This fixed point corresponds to the periodic solution given in equation (4.1). Using the numerical continuation software package AUTO-07P (see Doedel & Oldeman, 2007), we have computed the bifurcation diagram for this fixed point shown in Fig. 4. The parameter a is used as the continuation parameter; the other parameters are fixed at $(b, c, h, r, \omega) = (1, 1, 0.25, 3, 1)$. The fixed point is stable up to $a \approx 1.196$, where it loses stability in a supercritical pitchfork bifurcation. From the pitchfork bifurcation two stable fixed points emanate, which lose (resp. regain) stability at saddle-node bifurcations for $a \approx 1.233$ (resp. $a \approx 1.086$). After that the two branches undergo a period doubling bifurcation at $a \approx 1.175$. This leads to the coexistence of two stable period-2 points.

For $a \approx 1.197$ the stable period-2 points lose stability through a period doubling bifurcation that leads to the coexistence of two stable period-4 points. This suggests that an infinite cascade of period doubling bifurcations occurs when a increases. In principle, the next period doubling bifurcations can be obtained by means of numerical continuation. However, in a period doubling cascade the distances between successive period doublings asymptotically scale with the Feigenbaum constant $\delta \approx 4.669$ (see
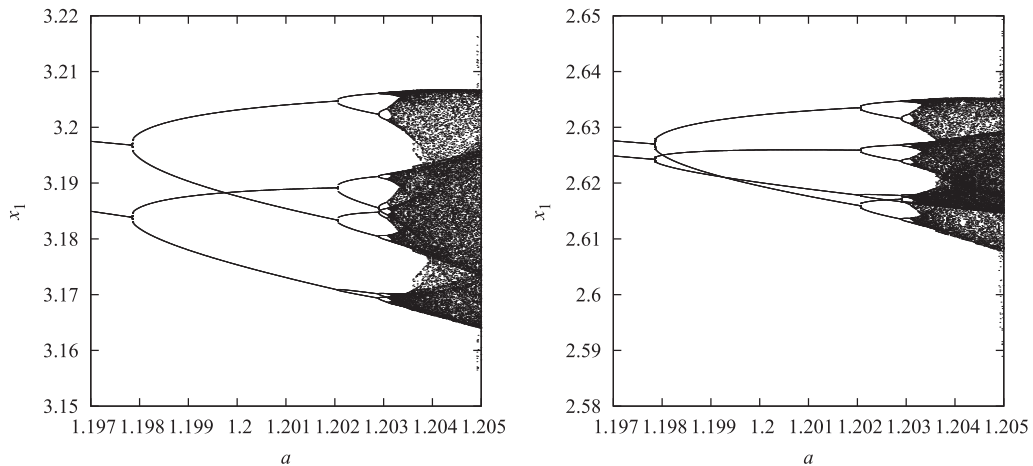
Fɪɢ. 5. Bifurcation diagram of two stable period-2 points of the Poincaré map $P : \Sigma \to \Sigma$. For each value of a the map P is iterated 500 times and the last 100 iterates are plotted. The parameters $(b, c, h, r, \omega) = (1, 1, 0.25, 3, 1)$ are fixed.

Guckenheimer & Holmes, 1983). This implies that prohibitively small step sizes are needed to detect the bifurcations by means of continuation. Bifurcations can go undetected when the step size is too large.

A more practical way of obtaining an overview of the dynamics of the Poincaré map P is to use brute force iteration. We increase the value of a from 1.197 up to 1.205 in 1000 steps. For each value of a we compute 600 iterates of P and plot the x_1-coordinates of the last 100 computed points as a function of a. The final point of the last attractor serves as an initial condition for the next loop. The starting points are the two stable period-2 points $(2.633, 0.00129)$ and $(3.203, 0.03657)$. The bifurcation diagrams for these points are shown in Fig. 5. This figure suggests that indeed each of the two points bifurcates through an infinite cascade of period doublings. In turn this leads to the coexistence of two chaotic attractors of which the structure will be discussed in the next section.

The coexistence of two or more attractors in a dynamical systems is referred to as *multi-stability*. This phenomenon often arises due to symmetries of the system (see Lai & Chen, 2016) and in particular due to the presence of pitchfork bifurcations (see Van Kekem & Sterk, 2017, 2018b) as is the case in the present paper. A different mechanism by which multi-stability can occur is due to the presence of codimension-2 bifurcations, such as double Hopf bifurcations (see Van Kekem & Sterk, 2018a). For an overview of the wide range of applications of multi-stability in different disciplines of science, see Feudel (2008).

4.3. *Chaotic dynamics*

Figure 6 shows two chaotic attractors of the Poincaré map $P : \Sigma \to \Sigma$ detected after the period doubling cascade. Note that these attractors coexist for the same parameter values. The attractors have the appearance of a 'fattened curve' that makes them qualitatively similar to the well-known attractor of the Hénon map (see Hénon, 1976). In fact, for the latter map it was proven by Benedicks & Carleson (1991) that for a set of parameter values with positive Lebesgue measure the attractor is the closure of the unstable manifold of a saddle fixed point.

By numerical continuation we obtained two saddle fixed points of the Poincaré map $P : \Sigma \to \Sigma$ for the parameter values $(a, b, c, h, r, \omega) = (1.205, 1, 1, 0.25, 3, 1)$. We computed the unstable manifolds of
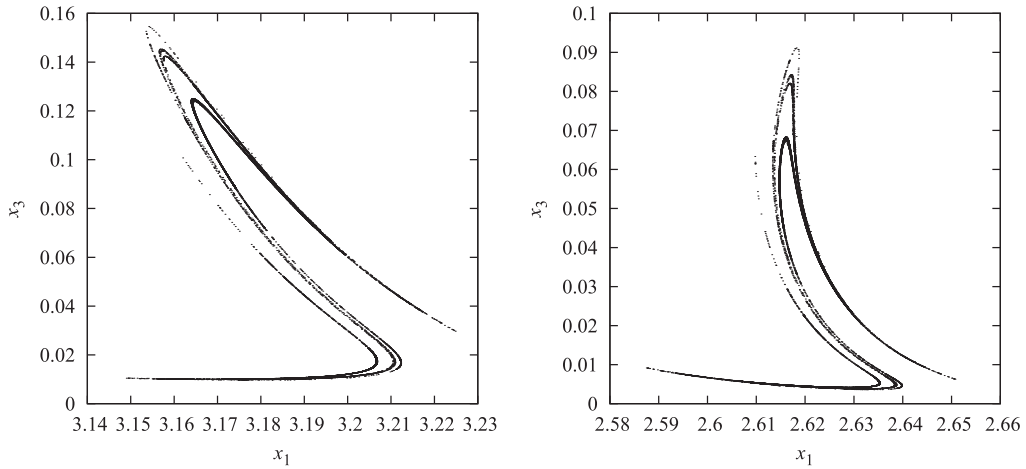
FIG. 6. Two coexisting chaotic attractors of the Poincaré map $P : \Sigma \to \Sigma$ for the parameter values $(a, b, c, h, r, \omega) = (1.205, 1, 1, 0.25, 3, 1)$. The corresponding attractors for the system (3.2) in $\mathbb{R}^3$ are shown in Fig. 8.
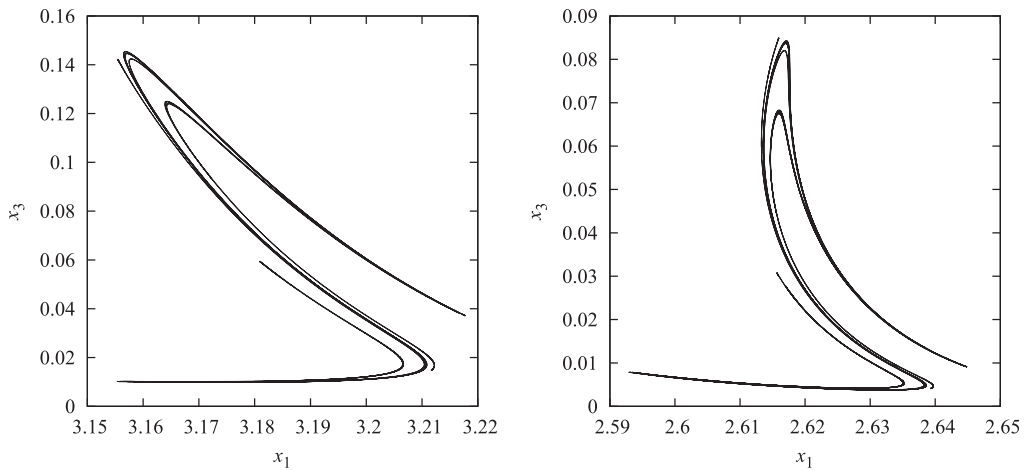
FIG. 7. Unstable manifold of two different saddle fixed points of the Poincaré map $P : \Sigma \to \Sigma$ for the parameter values $(a, b, c, h, r, \omega) = (1.205, 1, 1, 0.25, 3, 1)$. Note the striking resemblance with the attractors shown in Fig. 6.

these fixed points by means of techniques based on iterating fundamental domains described in Broer & Takens (2010) and Simó (1990). Their unstable manifolds are shown in Fig. 7. Note the striking resemblance with the attractors shown in Fig. 6. We therefore conjecture that these attractors are indeed the closure of the manifolds shown in Fig. 7. This implies that the corresponding chaotic attractors for the system (3.2) are the closure of the unstable manifold of a saddle periodic orbit.
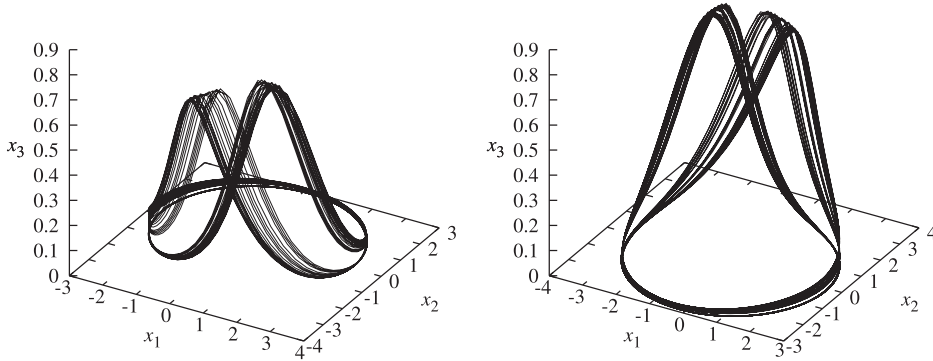
FIG. 8. Two coexisting chaotic attractors of the system (3.2) for the parameter values $(a, b, c, h, r, \omega) = (1.205, 1, 1, 0.25, 3, 1)$. Their corresponding Poincaré sections are shown in Fig. 6.

5. Control design

This section presents the possibility of using the eigenstructure analysis in non-linear control design. First, a non-linear state feedback controller is constructed to stabilize a chaotic system by the help of a NEValues assignment. Secondly, a synchronizing controller is obtained through a master-slave formalism.

5.1. *Chaos control*

The chaotic system (3.2) can be controlled just by one control input. In fact we can control the system in such a way that the origin becomes a global attractor by a single input u exerted on the x_3 component of the system (3.2) according to

$$
\begin{aligned}
\dot{x}_1 &= \left(x_3{}^2 - h^2\right) x_1 - \omega x_2, \\
\dot{x}_2 &= \omega x_1 + \left(x_3{}^2 - h^2\right) x_2, \\
\dot{x}_3 &= \left(r^2 - ax_1{}^2 - bx_2{}^2 - cx_3{}^2\right) x_3 + u.
\end{aligned}
\tag{5.1}
$$

The control function $u : \mathbb{R} \to \mathbb{R}$ makes the origin asymptotically stable if the following condition is satisfied:

$$
\lambda_{3cl}(\mathbf{x}) < 0 \quad \text{for all} \quad \mathbf{x} \in \mathbb{R}^3 \setminus \{\mathbf{0}\}.
\tag{5.2}
$$

From the eigenstructure analysis of the system depicted in Table 1 we see that even though the states x_1 and x_2 are not accessed by the input, the chaotic system can still be controlled by means of a simple state feedback of the form $u = -Kr^2 x_3$ with $K > 1$. The closed-loop system obtained by applying this controller is

$$
\begin{aligned}
\dot{x}_1 &= \left(x_3{}^2 - h^2\right) x_1 - \omega x_2, \\
\dot{x}_2 &= \omega x_1 + \left(x_3{}^2 - h^2\right) x_2, \\
\dot{x}_3 &\left((1 - K)r^2 - ax_1{}^2 - bx_2{}^2 - cx_3{}^2\right) x_3,
\end{aligned}
$$

which is again in PL form with the old NEValues $\lambda_{1,2_{cl}}(\mathbf{x}) = \lambda_{1,2}(\mathbf{x})$ and the new NEValue $\lambda_{3_{cl}}(\mathbf{x}) = (1-K)r^2 - ax_1{}^2 - bx_2{}^2 - cx_3{}^2$. The simulation results of this controlled system are illustrated in Fig. 9.

5.2. *Synchronization*

In this section we synchronize a pair of chaotic systems, which consist of a master system given by

$$\dot{x}_{m1} = \left(x_{m3}{}^2 - h^2\right)x_{m1} - \omega x_{m2},$$

$$\dot{x}_{m2} = \omega x_{m1} + \left(x_{m3}{}^2 - h^2\right)x_{m2},$$

$$\dot{x}_{m3} = \left(r^2 - ax_{m1}{}^2 - bx_{m2}{}^2 - cx_{m3}{}^2\right)x_{m3},$$

and a slave system given by

$$\dot{x}_{s1} = \left(x_{s3}{}^2 - h^2\right)x_{s1} - \omega x_{s2} + u_1,$$

$$\dot{x}_{s2} = \omega x_{s1} + \left(x_{s3}{}^2 - h^2\right)x_{s2} + u_2,$$

$$\dot{x}_{s3} = \left(r^2 - ax_{s1}{}^2 - bx_{s2}{}^2 - cx_{s3}{}^2\right)x_{s3} + u_3.$$

The equations for the error signal $\mathbf{e} = \mathbf{x}_s - \mathbf{x}_m$ are given by

$$
\begin{aligned}
\dot{e}_1 &= -h^2 e_1 - \omega e_2 + x_{s3}{}^2 x_{s1} - x_{m3}{}^2 x_{m1} + u_1, \\
\dot{e}_2 &= \omega e_1 - h^2 e_2 + x_{s3}{}^2 x_{s2} - x_{m3}{}^2 x_{m2} + u_2, \\
\dot{e}_3 &= r^2 e_3 - a\left(x_{s3}x_{s1}{}^2 - x_{m3}x_{m1}{}^2\right) - b\left(x_{s3}x_{s2}{}^2 - x_{m3}x_{m2}{}^2\right) - c\left(x_{s3}{}^3 - x_{m3}{}^3\right) + u_3.
\end{aligned}
\tag{5.3}
$$

Unfortunately, the synchronization of the master and slave system cannot be achieved by only one control input. Instead, we need three independent control inputs to guarantee that the origin of the system (5.3) is asymptotically stable. Hence, we consider the controller

$$
\begin{aligned}
u_1 &= -x_{s3}{}^2 x_{s1} + x_{m3}{}^2 x_{m1}, \\
u_2 &= -x_{s3}{}^2 x_{s2} + x_{m3}{}^2 x_{m2}, \\
u_3 &= -r^2 e_3,
\end{aligned}
$$

which gives the following closed-loop system for the error equations:

$$
\begin{aligned}
\dot{e}_1 &= -h^2 e_1 - \omega e_2, \\
\dot{e}_2 &= \omega e_1 - h^2 e_2, \\
\dot{e}_3 &= -a\left(x_{s3}x_{s1}{}^2 - x_{m3}x_{m1}{}^2\right) - b\left(x_{s3}x_{s2}{}^2 - x_{m3}x_{m2}{}^2\right) - c\left(x_{s3}{}^3 - x_{m3}{}^3\right).
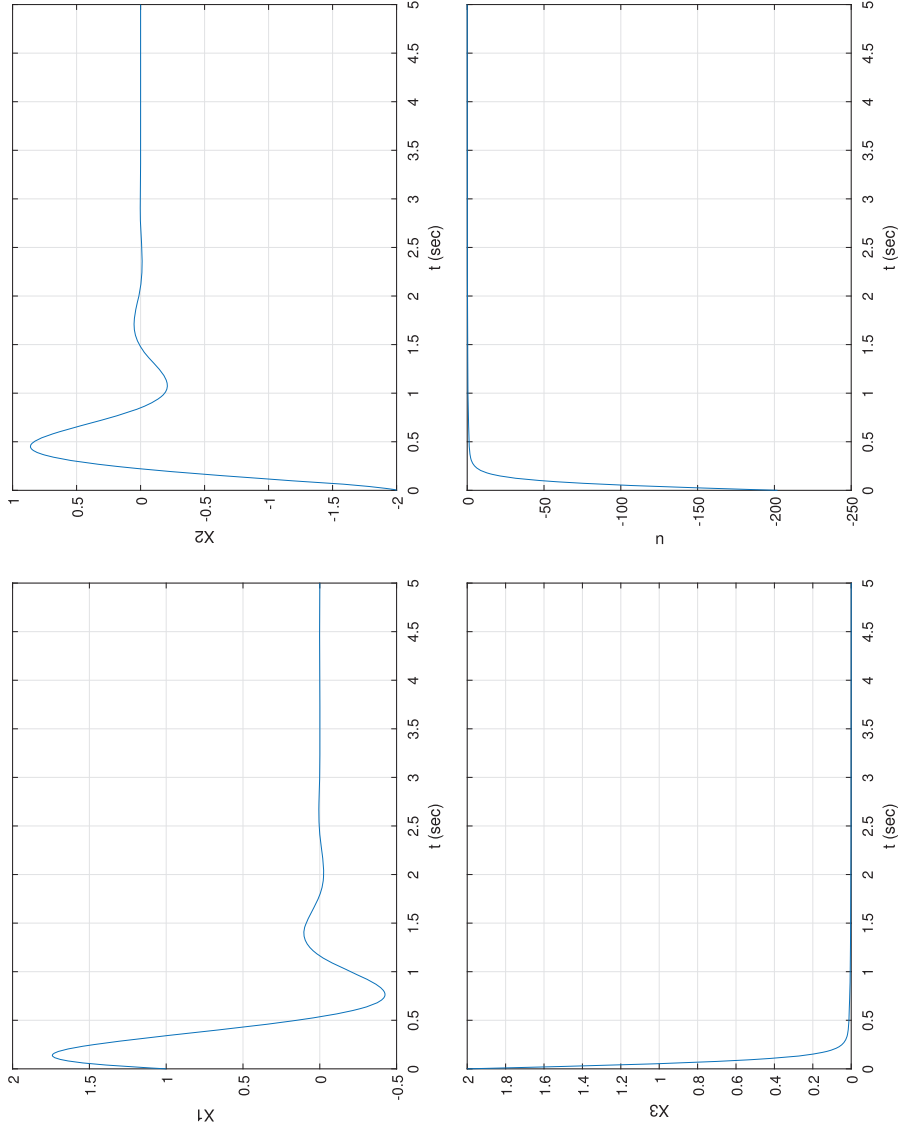\end{aligned}
$$

FIG. 9. Closed-loop results of system (5.1) with $u = -Kr^2x_3$ and $K = 1.1$ for the parameter values $(a, b, c, h, r, \omega) = (5, 1, 0.1, 1.5, 10, 5)$.
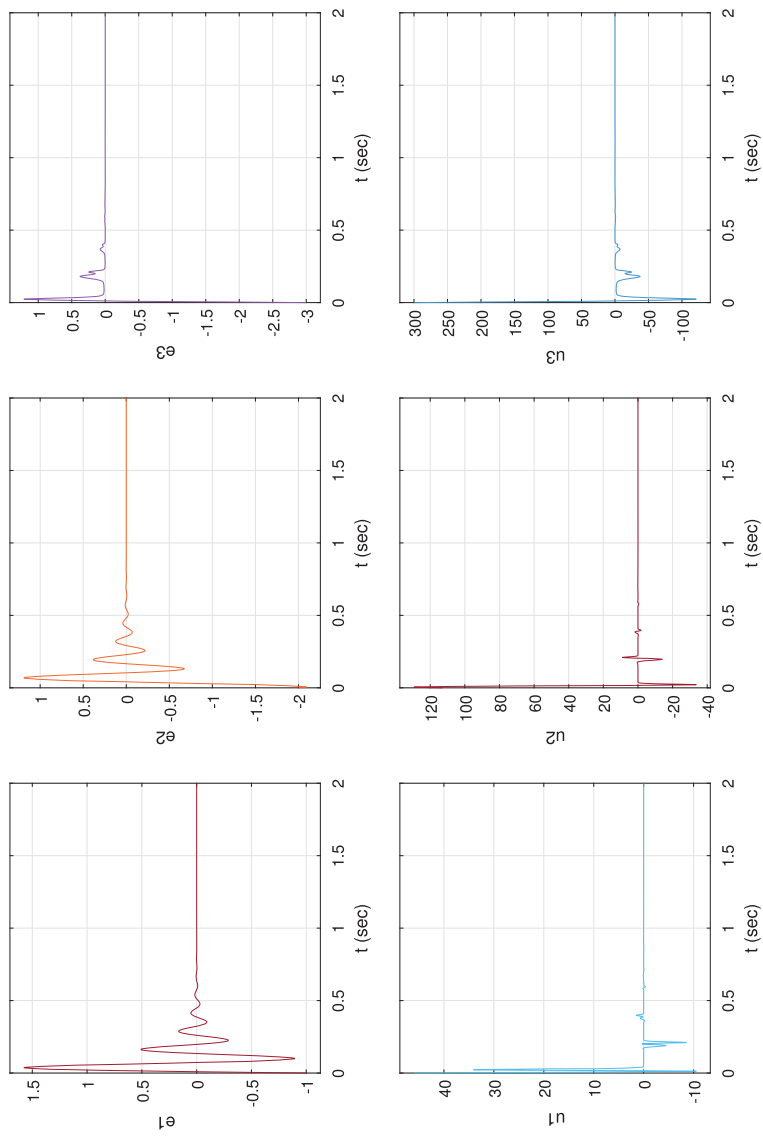
FIG. 10. Synchronization simulation results for the parameter values $(a, b, c, h, r, \omega, c) = (5, 1, 0.1, 4, 10, 50)$.

This means that regardless of e_3, the e_1 and e_2 components approach zero in a spiralling manner with the exponential rate of h^2. The remaining error dynamic in e_3 is then

$$\dot{e}_3 = -\left(ax_1^{*2} + bx_2^{*2} + c(x_{s3}^2 + x_{s3}x_{m3} + x_{m3}^2)\right)e_3,$$

in which x_1^* and x_2^* denote the synchronized values of x_1 and x_2 assuming that $e_{1,2}$ has saturated at 0. The dynamic of the e_3 component is in a PL form with the NEValue

$$\lambda_{3_{CL}}(\mathbf{e}) = -\left(ax_1^{*2} + bx_2^{*2} + c(x_{s3}^2 + x_{s3}x_{m3} + x_{m3}^2)\right).$$

Since $\lambda_{3_{CL}}(\mathbf{e}) \leq 0$, the asymptotic exponential stability of e_3 is guaranteed and then the complete synchronization of all components will be obtained. The simulation results are shown in Fig. 10.

It is worth mentioning that for the parameter values in both the control and synchronization simulations, system (3.2) is chaotic.

6. Concluding remarks

The key idea of this paper was to use the PL form representation of non-linear dynamical systems for the generation of chaotic behaviour. It is well known that the continual stretching and folding is the basic qualitative characteristic of a chaotic behaviour. This feature is essentially responsible for the local instability and global boundedness of chaotic trajectories. It has been shown that for a special class of non-linear dynamical systems, the NEValues are indicators for the qualitative behaviour of the system. These qualitative indicators were applied to synthesize a particular form of continual stretching and folding behaviour in the state space of a three-dimensional dynamical system. Numerical simulations verified the chaotic nature of the obtained system for a wide range of parameters. Chaotic dynamics arises through period doubling cascades of periodic attractors. Analysis by means of a Poincaré map suggests that the resulting chaotic attractors are of Hénon-like type, which means that they are the closure of an unstable manifold of a saddle periodic orbit. Due to symmetries the system also exhibits multi-stability, which means that two different chaotic attractors coexist for the same parameter values.

In addition, we showed that by means of an eigenstructure-based method the chaotic system can be easily both controlled and identically synchronized with another system through some non-linear state feedback even if not all states are accessible. We tried to show that some efforts in non-linear optimal control theory leading to the SDRE approach can be applied in another field of dynamical system theory. Currently, we are working on the definition and control of non-linear non-minimum phase system by the help of PL form representation and the results will be reported soon.

REFERENCES

BAILLIEUL, J. & WILLEMS, J. C. (1999) *Mathematical Control Theory*. New York: Springer.
BANKS, S. P. & MHANA, K. J. (1992) Optimal control and stabilization for nonlinear systems. *IMA J. Math. Control Inform*, **9**, 179–196.
BANKS, S. P. & MHANA, K. J. (1996) Pseudo-linear systems, Lie algebras, and stability. *IMA J. Math. Control Inform*, **13**, 385–401.
BENEDICKS, M. & CARLESON, L. (1991) The dynamics of the Hénon map. *Ann. of Math.*, **133**, 73–169.

BROER, H. W. & TAKENS, F. (2010) *Dynamical Systems and Chaos*. Applied Mathematical Sciences, vol. 172. New York: Springer.

CHENG, D., HU, X. & SHEN, T. (2010) *Linearization of Nonlinear Systems*. Analysis and Design of Nonlinear Control Systems. Berlin Heidelberg: Springer.

ÇIÇEK, S., FERIKOĞLU, A. & PEHLIVAN, I. (2016) A new 3D chaotic system: dynamical analysis, electronic circuit design, active control synchronization and chaotic masking communication application. *Optik*, **127**, 4024–4030.

ÇIMEN, T. (2008) State-dependent Riccati equation (SDRE) control: a survey. *IFAC Proc. Vol.*, **41**, 3761–3775.

CLOUTIER, J. R. (1997) State dependent Riccati equation techniques: an overview. *Proceedings of the American Controls Conference*, vol. 2. Albuquerque, NM, USA, USA: IEEE, pp. 932–936.

DOEDEL, E. J. & OLDEMAN, B. E. (2007) *AUTO–07p: Continuation and Bifurcation Software for Ordinary Differential Equations*. Montreal, Canada: Concordia University.

FEUDEL, U. (2008) Complex dynamics in multistable systems. *Int. J. Bifurcat. Chaos*, **18**, 1607–1626.

GHANE, H. & MENHAJ, M. (2014) Pseudo linear systems: stability analysis and limit cycle emergence. *J. Control Eng. Appl. Inform.*, **16**, 78–89.

GHANE, H. & MENHAJ, M. (2015) Eigenstructure-based analysis for non-linear autonomous systems. *IMA J. Math. Control Inform*, **32**, 21–40.

GUCKENHEIMER, J. & HOLMES, P. (1983) *Nonlinear Oscillations, Dynamical Systems and Bifurcations of Vector Fields*. Applied Mathematical Sciences, vol. 42. New York: Springer.

HÉNON, M. (1976) A two-dimensional mapping with a strange attractor. *Comm. Math. Phys.*, **50**, 69–77.

KUZNETSOV, Y. A. (2004) *Elements of Applied Bifurcation Theory*. Applied Mathematical Sciences, vol. 112. New York: Springer.

LAI, Q. & CHEN, S. (2016) Coexisting attractors generated from a new 4D smooth chaotic system. *Int. J. Control Autom. Syst.*, **14**, 1124–1131.

LANGSON, W. & ALLEYNE, A. (2002) A stability result with application to nonlinear regulation. *J. Dyn. Syst. Meas. Control*, **124**, 152–156.

MUHAMMAD, S. & VAN DER WOUDE, J. (2009) A counter example to a recent result on the stability of non-linear systems. *IMA J. Math. Control Inform.*, **26**, 319–323.

SCHÖLL, E. & SCHUSTER, H. G. (2008) *Handbook of Chaos Control*. Weinheim, Germany: John Wiley & Sons.

SIMÓ, C. (1990) On the analytical and numerical continuation of invariant manifolds. *Modern Methods in Celestial Mechanics* (D. Benest and C. Froeschlé eds). Gif-sur-Yvette: Éditions Frontières, pp. 285–330.

TSIOTRAS, P., CORLESS, M. & ROTEA, M. (1996) Counterexample to a recent result on the stability of nonlinear systems. *IMA J. Math. Control Inform*, **13**, 129–130.

VAN KEKEM, D.L. & STERK, A.E. (2017) Symmetries in the Lorenz-96 model. *Int. J. Bifurcat. Chaos.* In press.

VAN KEKEM, D. L. & STERK, A. E. (2018a) Travelling waves and their bifurcations in the Lorenz-96 model. *Phys. D*, **367**, 37–60.

VAN KEKEM, D. L. & STERK, A. E. (2018b) Wave propagation in the Lorenz-96 model. *Nonlinear Process. Geophys.*, **25**, 301–314.

WANG, B., ZHOU, S., ZHENG, X., ZHOU, C., DONG, J. & ZHAO, J. (2015) Image watermarking using chaotic map and DNA coding. *Optik*, **126**, 4846–4851.

ZANG, X., IQBAL, S., ZHU, Y., LIU, X. & ZHAO, J. (2016) Applications of chaotic dynamics in robotics. *Int. J. Adv. Robot. Syst.*, **13**, 1–17.

ZHOU, Y., BAO, L. & PHILIP, C. L. (2014) A new 1D chaotic system for image encryption. *Signal Process.*, **97**, 172–182.